Journal of Zhejiang University-SCIENCE C (Computers & Electronics)
ISSN 1869-1951 (Print); ISSN 1869-196X (Online)
www.zju.edu.cn/jzus; www.springerlink.com
E-mail: jzus@zju.edu.cn

Optimization of the resonant frequency servo loop technique in the resonator micro optic gyro*

Yang REN†, Zhong-he JIN†‡, Yan CHEN, Hui-lian MA

(*Department of Information Science & Electronic Engineering, Zhejiang University, Hangzhou 310027, China*)

†E-mail: zju.renyang@qq.com; jinzh@zju.edu.cn

Received Dec. 26, 2010; Revision accepted Apr. 1, 2011; Crosschecked Aug. 29, 2011

Abstract: Proportional integrator (PI) is always adopted in the resonant frequency servo loop in a resonator micro optic gyro (RMOG). The oscillation phenomenon is observed when adjusting the loop gain surpassing a threshold. This phenomenon limits system performance on step response speed and residual error. Based on the experiment system, a simulation model was set up. Further analysis shows that the threshold gain is related to the system loop filter setting and the loop delay. The traditional PI frequency servo loop technique in the RMOG system cannot keep up with the environment's disturbance quickly enough, which leads to a large residual error. A compensating method is proposed to optimize the tracking performance, solve the oscillation problem, and speed up the system response. Simulation and experiment results show that the compensated system is superior in performance. It has less residual error in the stable state and is 10 times quicker than the uncompensated system on the step response.

Key words: Resonator micro optic gyro (RMOG), Resonance frequency servo loop, Phase compensating method
doi:10.1631/jzus.C1000441 **Document code:** A **CLC number:** TN24

1 Introduction

Optical gyros based on the Sagnac effect (Post, 1967) are the best choice for an inertial navigation system. Resonator optic gyro (ROG) has been studied since the 1970s. Two kinds of ROG, resonator fiber optic gyro (RFOG) (Ezekiel and Balsamo, 1977; Sanders *et al*., 1981) and resonator micro optic gyro (RMOG) (Iwatsuki *et al*., 1984; Ma *et al*., 2009), have been proposed to reduce the fiber length and the gyro size when compared to the interferometric fiber optic gyro (IFOG) (Vali and Shorthill, 1976; Leeb *et al*., 1979). With the development of integrated optical technology (Iwatsuki *et al*., 1989; Suzuki *et al*., 2000; Hsiao and Winick, 2007; Vannahme *et al*., 2007), RMOG has gradually become a promising candidate gyro, with the advantages of low cost, compact nature, and vibration immunity.

In both types of resonator gyros, the rotation rate readout is given as the resonant frequency difference between the clockwise (CW) and counterclockwise (CCW) lightwaves propagating in the ring resonator through the Sagnac effect. The resonant frequency difference introduced by the Sagnac effect is much smaller than the temperature fluctuation induced drifts. Most of the readout methods of ROGs are based on the phase modulation spectroscopy technique, such as the sinusoidal phase modulation (Sanders *et al*., 1981; Ma *et al*., 2006; 2009; 2011; Zhang *et al*., 2006; Mao *et al*., 2011), the digital serrodyne modulation (Hotate and Harumoto, 1997), the digital triangular signal modulation (Ying *et al*., 2008), the binary phase shift keying modulation (Hotate *et al*., 1990), and the ternary phase shift keying method (Suzuki *et al*., 1999). In the sinusoidal phase modulation technique, the modulation frequency is limited only by the cutoff frequency of the

‡ Corresponding author

* Project supported by the National High-Tech R & D Program (863) of China (No. 2008AA042602) and the Fundamental Research Funds for the Central Universities, China (No. KYJD09035)

phase modulator, which can reach hundreds of MHz to several GHz. It is the best choice for the RMOG (Zhang *et al*., 2006). A resonant frequency servo loop, which is used to make the central frequency of the laser source to track the resonance of the ring resonator in one direction, is necessary in the resonator gyros. When the laser frequency maintains the resonance of the ring resonator in one direction, for example, the CCW lightwave, the frequency difference between the laser frequency and the other resonant frequency of the ring resonator is used as the open-loop readout of the rotation rate.

Proportional integrator (PI) is usually adopted in the resonant frequency servo loop for the laser frequency to eliminate the residual error at the frequency of the lock-in detection, which is used to demodulate the output from the resonator. A high loop gain is preferred to achieve a small residual error. In a practical RMOG system, unusual effects have been observed in the process of tracking the resonant frequency. The system output shows an oscillation problem when the loop gain exceeds a threshold, which limits the system performance. Further analysis shows that the threshold gain is related to the system loop filter setting and the loop delay of the RMOG. The traditional frequency servo loop technique in the RMOG system cannot respond to the temperature disturbance quickly enough, thus leading to a larger residual error and a longer lock-in transition state. Based on the experiment system, the simulation model for the resonant frequency servo loop, which is used to analyze the oscillation phenomenon in the RMOG system, is first set up. Moreover, we propose the compensating method to optimize the closed-loop tracking performance, solve the oscillation problem, and speed up the system response, based on the analytical model.

2 Experimental

Fig. 1 shows the setup of the RMOG system based on the sinusoidal phase modulation technique (Ma *et al*., 2009; 2011; Mao *et al*., 2011). All the fibers in the system are polarization maintaining.

The lightwave from a fiber laser (FL) (linewidth less than 50 kHz) is equally divided by coupler C1, and injected into the silica waveguide ring resonator

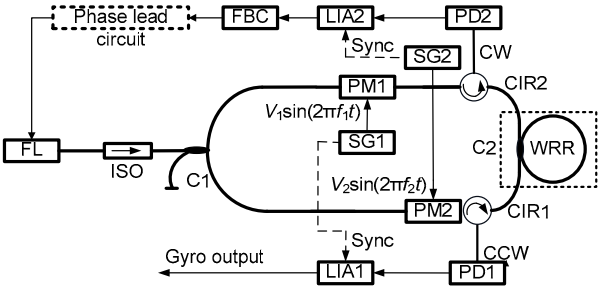

Fig. 1 RMOG experiment system apparatus

FL: fiber laser; ISO: isolator; C1, C2: couplers; PM1, PM2: phase modulators; SG1, SG2: signal generators; CIR1, CIR2: circulators; WRR: waveguide ring resonator; PD1, PD2: photodetectors; LIA1, LIA2: lock-in amplifiers; FBC: feedback circuit; CW: clockwise; CCW: counterclockwise; V_1: amplitude of sine signal generated by SG1; V_2: amplitude of sine signal generated by SG2; Sync: synchronous signal from SG1 to LIA1, SG2 to LIA2

(WRR) in the CW and the CCW lightwaves. The total ring length of the WRR is 7.9 cm. Phase modulators PM1 and PM2 are driven by sinusoidal waveforms from signal generators SG1 and SG2 with modulation frequencies f_1 and f_2, respectively. The CCW and CW lightwaves from the silica WRR are detected by the InGaAs PIN photodetectors PD1 and PD2, respectively. The output of the PD2 is fed back through the lock-in amplifier LIA2 to the feedback circuit (FBC) to cancel fluctuations in resonant frequency and/or the central frequency of the FL. A PI is adopted in the FBC to eliminate the residual error at the lock-in frequency. The demodulated signal of the CCW lightwave from LIA1 is used as the open-loop monitor of the rotation rate.

A sawtooth wave voltage tunes the central frequency of the FL linearly with respect to time. The resonance curves for the CW and CCW lightwaves of the silica WRR are detected by the photodetectors PD2 and PD1, respectively. Fig. 2a shows the measured results for the CCW lightwave. The measured full width at half maximum (FWHM) is about 56.3 MHz. The free spectrum range (FSR) of the silica WRR is 2.61 GHz. Fig. 2b shows the demodulation curve measured at LIA1 for the CCW lightwave. The gain of LIA1 is about 800 a.u. The slope of the demodulation curve for the linear part with unit gain is 7.29 nV/Hz. This figure stands for the optical gain of the system. The maximum range of resonance frequency difference corresponding to the linear

region is ±23.67 MHz. To form a closed-loop operation, the output of LIA2 is fed back through the FBC to the laser controlling panel to adjust the central frequency of the FL. Fig. 3 shows the transition state of the lock-in process. A sinusoidal signal with the frequency of 18 MHz is observed at LIA2 under the lock-in state because a 9 MHz modulation signal is applied to PM2 (Ma *et al*., 2006). A bias stability of the experiment system is 1.7×10^{-2} rad/s over 500 s with an integration time of 0.3 s (Mao *et al*., 2011).

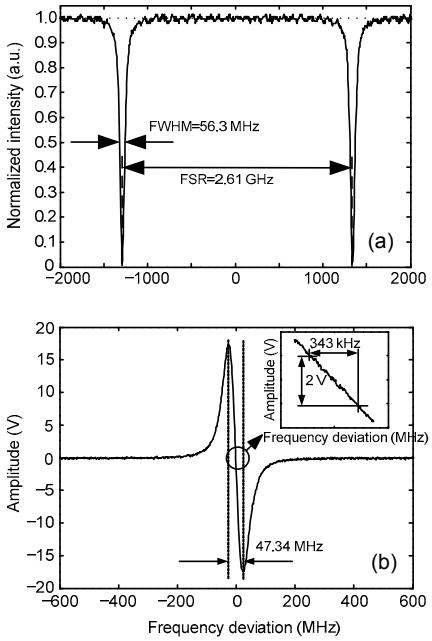

Fig. 2 Frequency response of the silica waveguide ring resonator (a) and the demodulation curve (b) of the counterclockwise lightwave

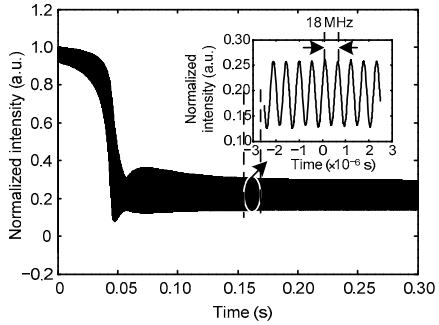

Fig. 3 Closed-loop transition state in the lock-in progress

The system loop gain is adjusted from low to high in order to make the system have a quicker response and less residual error. In the experiment, a gain threshold was observed, which is related to the system loop filter setting and the loop delay. When the system loop gain is larger than the threshold, the output of LIA1 will oscillate, showing the instability of the closed loop. Fig. 4 gives the experimental results of the open-loop output of the RMOG in the normal (solid line) and oscillating (dashed line) states, respectively. The oscillation frequency is 363.32 Hz. The normal system open-loop output fluctuation is generated by poor locked loop and nonreciprocal optical noise, such as backscattering noise, Kerr effect noise, and polarization noise.

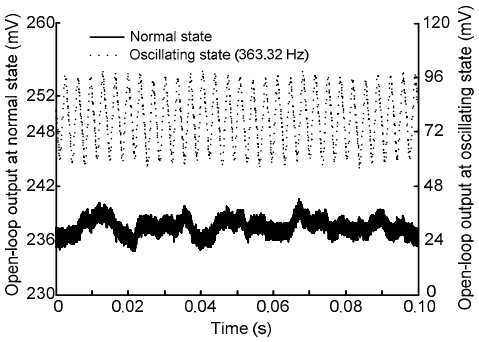

Fig. 4 Amplitude of the open-loop output at normal and oscillation states

According to the closed-loop control theory (Ogata, 2003), a high closed-loop gain means a quicker step response and less residual error. The traditional frequency servo loop in the RMOG cannot respond to the system disturbance quickly enough, thus leading to a huge residual error. The normal servo loop system performance is limited by the gain threshold problem.

3 System loop analysis and simulation

3.1 System loop model

Few papers refer to the resonant frequency servo loop techniques in the RMOG. An original analytical model is proposed to analyze the system performance and explain the oscillation problem. Fig. 5 shows the *s*-domain analytical model including two separate loops: closed loop and open loop. The closed-loop feeds back the output signals of LIA2 through the FBC to track the resonant frequency of WRR. The output signal of the open loop is used as the readout of gyro rotation rate, affected by the performance of the closed loop. In Fig. 5, parameters k_{pd}, k_l, and k_{laser} are

the gain of the whole optical path, the gain of the LIA, and the voltage modulation index of the FL, respectively. Block servo stands for the loop filter for the tracking loop, which includes two parts: the low-pass filter of LIA2 and the FBC. Block filter is the open-loop output low-pass filter. In system model construction, the most important simplification is taking the optical signal processing, including the phase modulation, resonance in WRR, and lock-in demodulation, as a gain, which has proved accurate enough.

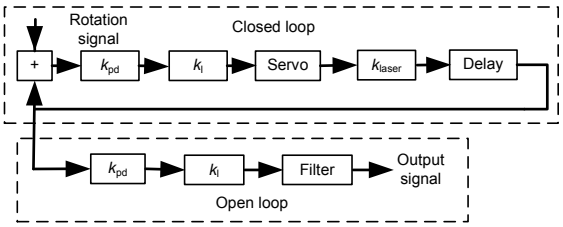

Fig. 5 System loop model

k_{pd}: gain of the whole optical path; k_l: gain of the LIA; k_{laser}: voltage modulation index of the FL

The transfer function for the CCW lightwave optical path in an open condition is

$$H_{\text{open}} = k_{\text{PD}} H_{\text{PD}} k_{\text{l}} H_{\text{servo}} k_{\text{laser}} H_{\text{laser}} H_{\text{D}}, \tag{1}$$

where H_{PD}, H_{servo}, H_{laser}, and H_{D} are the transfer functions of PD, servo loop, laser, and system delay item, respectively. H_{PD} is working as a low-pass filter whose equation is written as

$$H_{\text{PD}} = \frac{1}{s/(2\pi f_{\text{cut-off}})+1}, \tag{2}$$

where $f_{\text{cut-off}}$ is the 3 dB cutoff frequency of the PD, which is related to the PD gain setting. In our experiment system, $f_{\text{cut-off}}$ is 10 MHz. s is the Laplace operator. The servo loop transfer function H_{servo} is

$$H_{\text{servo}} = \frac{1}{Ts+1} k_{\text{c}} \frac{T_{\text{i}} s+1}{T_{\text{i}} s}. \tag{3}$$

In Eq. (3), the first part is the transfer function of the Butterworth low-pass filter in LIA2:

$$H_{\text{Butterworth}} = \frac{1}{Ts+1}, \tag{4}$$

where T is the time constant of the low-pass filter. The second part marked as H_{PID} is the transfer function of the PI unit, expressed as

$$H_{\text{PID}} = k_{\text{c}} \left(1 + \frac{1}{T_{\text{i}} s}\right), \tag{5}$$

where k_{c} and T_{i} represent the voltage gain and the integration time of the PI unit, respectively.

The central frequency of the FL is controlled by adding a voltage on the piezoelectric ceramics (PZT). Because of the 2 μF capacitance on the laser voltage input port, the responses of the FL are considered as a low-pass filter with a 3 dB bandwidth of 1.6 kHz. The transfer equation of the FL is

$$H_{\text{laser}} = \frac{1}{T_{\text{laser}} s+1}, \tag{6}$$

where T_{laser} is the filter time constant of the FL. T_{laser} is related to the 3 dB bandwidth of the low-pass filter. In experimental setting, T_{laser} is 99.47 μs, making the pole of Eq. (6), $s=-1.0054\times10^4$, which is far from H_{servo} (T=1, k_{c}=1, T_{i}=0.024) zero $s=-41.67$ and poles s=0 and $s=-1$. H_{servo} zeros and poles can be treated as the dominant zeros and poles (Ogata, 2003) in analysis. The H_{laser} equation can be traded as a delay item, rewritten as

$$H_{\text{laser}} = \mathrm{e}^{-T_{\text{laser}} s}. \tag{7}$$

H_{D} is expressed as

$$H_{\text{D}} = \mathrm{e}^{-T_{\text{d}} s}, \tag{8}$$

where T_{d} is the total loop delay, including the system processing time, transmitting delay, and processing group delay induced by the loop filter. In the experiment, the Stanford SR844 works as the LIA. SR844 is a digital-analog mix system. The total delay of SR844 is about 82.69 μs, the analog 7th order active Cauer filter with a corner frequency of 18 kHz contributing 61.86 μs processing group delay. The digital part of the working clock in SR844 is 48 kHz, inducing a 20.83 μs processing delay. The digital equipment PI, which is set up by the National

Instrument (NI) DAQ board and Labview software in Windows platform, contributes 500 μs processing time delay because of the low sampling rate limited by the operating system. Compared with the process time and group delay, the optical path transmitting delay of 10 ns is small enough to be neglected.

Laser equation H_{laser}, SR844 delay, and NI DAQ delay, the three items constitute the whole loop delay of 682.16 μs.

3.2 System open-loop state analysis

Substituting Eqs. (1), (2), and (4)–(8) into Eq. (3) and replacing s by j2πf, we can obtain the Bode plot for the experimental system as shown in Fig. 6. Abs(H) is the amplitude frequency plot. Arg(H) is the phase frequency plot. The angular frequency of 2284 rad/s whose system frequency gain is 0.7 has a phase shift of −180° (Fig. 6). It is clear that the system gain margin is very small, only 3.1 dB. If the system gain is increased by more than 3.1 dB making gain at 2284 rad/s larger than 1, the system will be unstable (Ohtsu and Tabuchi, 1988) and will show oscillation sinusoidal wave similar to Fig. 4.

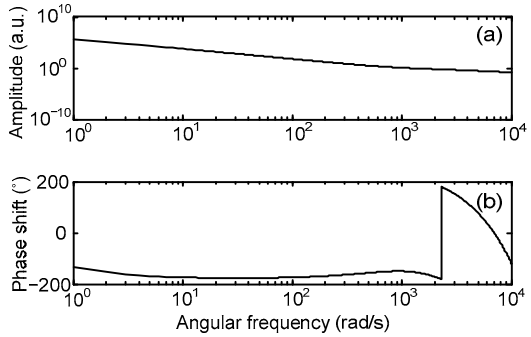

Fig. 6 System Bode plot
(a) Amplitude-frequency response, Abs(H); (b) Phase-frequency response, Arg(H)

We cannot improve system performance only by increasing loop gain because of the low gain margin. If we continue to increase the system gain beyond the threshold, the system will resonate at an angular frequency of 2284 rad/s (363.5 Hz). The oscillation frequency perfectly matches the system experimental result in Fig. 4. The system is sensitive to environmental disturbance. The system phase margin is small below 2284 rad/s. A large disturbance would make the system unstable.

3.3 System frequency response and step response analysis

From Eq. (3), the system closed-loop transfer function (Franklin *et al*., 2007), H_{close}, can be written as

$$H_{\text{close}}=\frac{H_{\text{open}}}{1-H_{\text{open}}}. \tag{9}$$

With H_{open}, H_{close} is rewritten as

$$H_{\text{close}}=\frac{s\left(2\xi\omega_{\text{n}}-\omega_{\text{n}}^2/k\right)+\omega_{\text{n}}^2}{s^2+2s\xi\omega_{\text{n}}+\omega_{\text{n}}^2}, \tag{10}$$

where

$$k=k_{\text{PD}}k_{\text{l}}k_{\text{laser}}k_{\text{c}}/T_{\text{i}},\ \ \omega_{\text{n}}=\sqrt{k/\tau_1},$$
$$\xi=\frac{1}{2}\sqrt{k/\tau_1}\left(\tau_2+\frac{1}{k}\right),\ \ \tau_1=T,\ \ \tau_2=T_{\text{i}},$$

k, ω_{n}, and ξ are the loop gain, natural angular frequency, and system damping ratio, respectively. Using inverse Laplace transform on Eq. (10), we obtain the system step response in time-domain value:

$$y(t)=-\Delta f\frac{2\xi\omega_{\text{n}}-\omega_{\text{n}}^2/k}{2\omega_{\text{n}}\sqrt{\xi^2-1}}\left(\mathrm{e}^{\omega_{\text{n}}t\left(\sqrt{\xi^2-1}-\xi\right)}-\mathrm{e}^{\omega_{\text{n}}t\left(-\sqrt{\xi^2-1}-\xi\right)}\right)$$
$$-\Delta f\left[1+\frac{1}{2}\frac{1}{\xi^2-1-\xi\sqrt{\xi^2-1}}\mathrm{e}^{\omega_{\text{n}}t\left(\sqrt{\xi^2-1}-\xi\right)}\right.$$
$$\left.+\frac{1}{2}\frac{1}{\xi^2-1+\xi\sqrt{\xi^2-1}}\mathrm{e}^{\omega_{\text{n}}t\left(-\sqrt{\xi^2-1}-\xi\right)}\right],\ \ \xi>1, \tag{11}$$

$$y(t)=-\Delta f\frac{2\xi\omega_{\text{n}}-\omega_{\text{n}}^2/k}{2\mathrm{j}\omega_{\text{n}}\sqrt{1-\xi^2}}\left(\mathrm{e}^{\omega_{\text{n}}t(\mathrm{j}\sqrt{1-\xi^2}-\xi)}-\mathrm{e}^{\omega_{\text{n}}t(-\mathrm{j}\sqrt{1-\xi^2}-\xi)}\right)$$
$$-\Delta f\left\{1-\frac{\mathrm{e}^{-\xi\omega_{\text{n}}t}}{1-\xi^2}\left[(1-\xi^2)\cos(\omega_{\text{n}}t\sqrt{1-\xi^2})\right.\right.$$
$$\left.\left.+\xi\sqrt{1-\xi^2}\sin(\omega_{\text{n}}t\sqrt{1-\xi^2})\right]\right\},\ \ \xi<1, \tag{12}$$

$$y(t)=-\Delta f\left(2\omega_{\text{n}}-\omega_{\text{n}}^2/k\right)t\mathrm{e}^{-\omega_{\text{n}}t}$$
$$-\Delta f(1-\mathrm{e}^{-\omega_{\text{n}}t}-\omega_{\text{n}}t\mathrm{e}^{-\omega_{\text{n}}t}),\ \ \xi=1. \tag{13}$$

Keeping ω_{n} unchanged, the system step response with different ξ can be drawn (Fig. 7). The plot shows that,

although a larger damping ratio leads to a quicker response, which is different from the classic two-order loop filter, a larger damping ratio requires more time to make the residual error small enough, e.g., 0.1% error of disturbance signal. We can see that adjusting the damping ratio distinctly affects overshoot and oscillation in the step response. The overshoot hits 20% within 0.015 s of the oscillation cycle when the damping ratio is 0.733, while the system reaches its best performance when the ratio is 0.978. The system takes only 0.022 s to reach a 2% error and 0.025 s to reach 1%. At the same time, the system attenuates 20 dB every 0.01 s. Continuously increasing the damping ratio, for example, to 5.796, the system seems to be efficient at first, but extremely inefficient when it reaches 1% error. The attenuating speed is almost every 0.09 s, attenuating 20 dB.

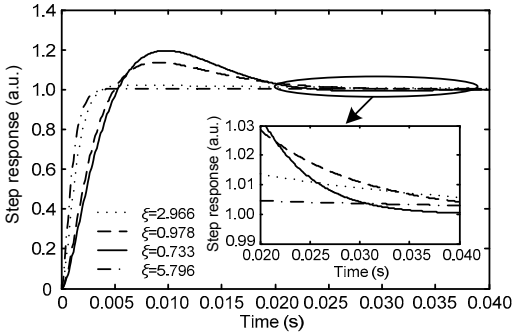

Fig. 7 System step response with different damping ratios

Fig. 8 shows the damping ratio versus response time with 0.1% error of disturbance signal. The step response time first decreases with the increase in the damping ratio, and then it begins to rise at ξ=0.978, which is the best selection for the experiment system settings, with the minimum value of 35 ms. The poor damping ratio ξ selection will limit the tracking speed under the environment fluctuations. With an improper damping ratio, the step response time will rapidly increase. A damping ratio of 0.3 corresponds to 0.1 s, while 5 corresponds to 0.09 s. The proper damping ratio of 0.9 has a step response time of 0.032 s, leading to a threefold enhancement compared to the damping ratio of 0.3.

In fact, the response time at ξ=0.978 is still not fast enough. The resonating frequency changes by 120 MHz when the temperature changes by 0.1 °C. The system scale factor is 10 mV/(°/s), and the 1°/s rotating signal generates a 194 Hz resonating frequency difference. All of these mean that even a small temperature change will cause the output to change significantly. In Table 1, the error frequency change over time is listed in simulation for ξ=0.978. Clearly, when temperature changes by 0.02 °C, the resonant frequency changes by 20 MHz, requiring about 150 ms for the error frequency to reduce to 1 kHz, which induces 51.5 mV biases at the gyro output. Seriously, a temperature change of 10^{-6} °C will generate a 1 kHz resonance frequency deviation. To achieve a more stable and robust system, we need a quicker system response to decrease the environmental fluctuation. Aimed at this, a compensating method is proposed in the ROG system.

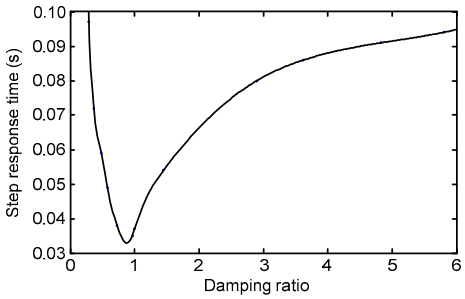

Fig. 8 Simulation results: 0.1% error step response time changes with the damping ratio

Table 1 Comparison of error frequency change with time between the compensated and uncompensated systems

Error/Initial frequency ($\times10^{-6}$)	Uncompensated time (s)	Compensated time (s)
9300	0.027 48	0.008 563
4600	0.043 64	0.011 680
46	0.151 00	0.020 320
4.6	0.204 70	0.024 590
0.046	0.312 10	0.033 060

3.4 Compensating method

From the above analysis, we can conclude that the system performance cannot be improved by simply increasing loop total gain, because of the large loop delay of 680 μs. If we continue increasing the loop gain, the system will oscillate at about 360 Hz. To solve the oscillation problem and make the system response quicker, a compensating method is proposed by inserting a phase lead circuit unit H_{com} into the FBC in the RMOG system. H_{com} is effective in making up the system phase margin in the low-frequency domain and leads to a quicker system response. The

H_{com} equation is

$$H_{\text{com}}(s)=\frac{s+\omega_{\text{com}}\sqrt{k_{\text{com}}}}{s+\omega_{\text{com}}/\sqrt{k_{\text{com}}}}, \tag{14}$$

where ω_{com} is the compensated angular frequency related to system loop filter settings and loop delay. k_{com} decides how much phase is compensated at ω_{com}. In simulation, we set ω_{com}=1398 rad/s, k_{com}=0.4 and plot the system step response with and without the compensating method. With k_{com}=0.4, the closed loop will achieve a 25.4° compensating angle at 1398 rad/s (Ogata, 2003). Fig. 9 shows the schematic diagram of the suggested phase lead circuit, being the compensating circuit block.

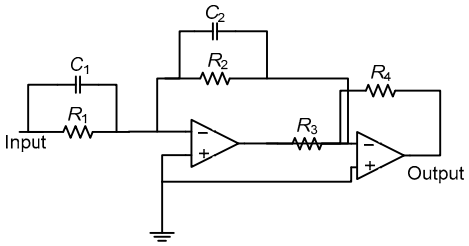

Fig. 9 Phase lead circuit

$k_{\text{com}}=R_2C_2/(R_1C_1)$, $R_4/R_3=C_2/C_1$, $\omega_{\text{com}}=(R_1R_2C_1C_2)^{-0.5}$

Fig. 10 gives the system performance comparisons between the uncompensated and compensated conditions. The system step response transition state is shown in Fig. 10a. The compensated system has a quicker response under the same loop delay compared with the uncompensated one. Although the overshoot increases by 20% compared to the uncompensated system, the time to reach 1% error falls from 0.027 to 0.0085 s. Fig. 10b shows the temperature variation of the WRR, which is used as a fluctuation source in simulation to compare system performance differences between uncompensated and compensated conditions. To reduce the influences of the ambient air flow and temperature, the WRR is placed in a thermal insulation box. The temperature of the WRR is tested by the temperature transducer under laboratory conditions. The test results show that the temperature variation of the ring resonator is stabilized within 0.03 °C for 50 s with this box. The temperature fluctuation has a peak-to-peak value of 0.03 °C and the largest gradient of 0.0024 °C/s. The gradient value

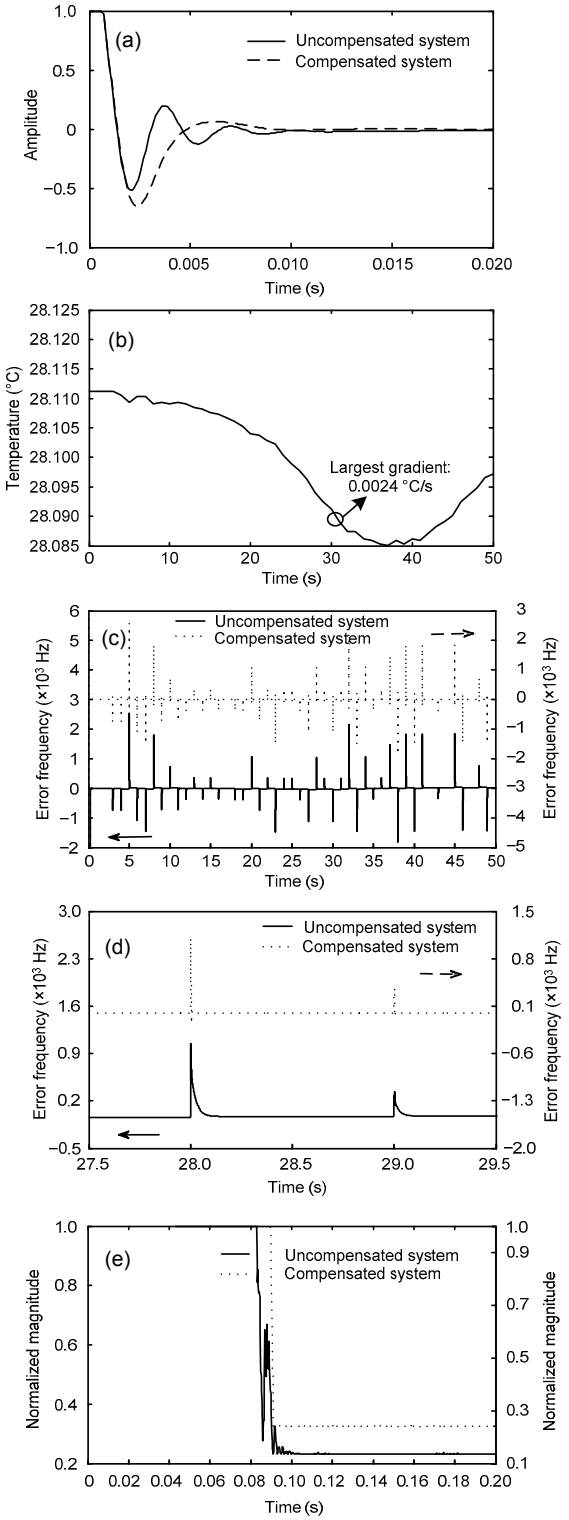

Fig. 10 System performance comparisons between the uncompensated and compensated conditions

(a) Step response; (b) Temperature variation with time; (c)–(d) Simulation results of the residual error at the lock-in frequency responding to temperature disturbance; (e) Experiment results with the transition process

causes a 2 MHz frequency shift. Figs. 10c and 10d show the simulation results of the residual error at the lock-in frequency responding to this temperature variation. The system closed loop tries to track the temperature change to satisfy the resonance condition when the temperature changes. The compensated system uses less time to relock from this temperature disturbance and produces less residual frequency error at the stable state, showing better performance. Fig. 10d shows the system response at 27.5 to 29.5 s, showing a lower residual error and quicker response for the compensated system. System response speed changes every 0.005 s, attenuating 20 dB, compared to the uncompensated system's every 0.02 s attenuating 20 dB. The closed loop becomes stable more quickly with the compensating method after a transition state period. The comparison of error frequency change with time between the compensated and the uncompensated systems is listed in Table 1. The compensated system requires only 10% as much of the time required by the uncompensated system to bring the error frequency below 0.046×10^{-6} of the initial frequency deviation. Fig. 10e shows the experiment results of the lock-in process comparisons between the uncompensated system and the compensated system. Although the experiment results are not as good as the simulation results shown in Fig. 10d for the limited resolution of the oscilloscope, they still obviously show the great advantages of the compensated system in quicker transition state speed and stabilization. As we see, the oscillation process for the uncompensated system contains multiple cycles of up and down with an overshoot of 0.65, an oscillation cycle of 0.002 s, and every 0.0126 s attenuating 3 dB. The uncompensated system uses 0.0172 s to reach 1% error compared to 0.0052 s for the compensated system.

The simulation we carry out to compare the normal system with the compensated system shows great improvement in step response performance. The compensated method has four benefits. First, the system has more gain margin and phase margin with the same system loop delay compared to the uncompensated system. Second, the compensated system response to temperature disturbance is quicker. Third, the compensated system has a more stable response transition state. Finally, the compensated system has less residual error in the stable state.

4 Conclusions

In this RMOG experiment, a system oscillation phenomenon is observed when the loop gain exceeds a threshold. The system performance is limited by the threshold and the system cannot respond to environmental fluctuation rapidly enough. Based on the experiment, an analytical model was built. It is shown that the oscillation problem strongly depends on loop delay and the closed-loop filter setting. Experiment and simulation results demonstrate that the ordinary RMOG system servo loop step response is not quick enough to track the resonance frequency change caused by system fluctuation. To handle this problem, a compensated method based on the analytical model is proposed and is superior to the traditional uncompensated system. With the compensated method, the RMOG system servo loop has a tenfold greater step response speed and less residual error under the stable state compared to the uncompensated method. The experiment results also exhibit great advantages of the compensated system in both transit state speed and stabilization.

References

Ezekiel, S., Balsamo, S.R., 1977. Passive ring resonator laser gyroscope. *Appl. Phys. Lett.*, **30**(9):478-480. [doi:10.1063/1.89455]

Franklin, G.F., Powell, J.D., Emami-Naeini, A., 2007. Feedback Control of Dynamic Systems (5th Ed.). Pearson Education, NJ, USA, p.314-412.

Hotate, K., Harumoto, M., 1997. Resonator fiber optic gyro using digital serrodyne modulation. *J. Lightwave Technol.*, **15**(3):466-473. [doi:10.1109/50.557562]

Hotate, K., Takiguchi, K., Hirose, A., 1990. Adjustment-free method to eliminate the noise induced by the backscattering in an optical passive ring-resonator gyro. *IEEE Photon. Technol. Lett.*, **2**(1):75-77. [doi:10.1109/68.47048]

Hsiao, H.K., Winick, K.A., 2007. Planar glass waveguide ring resonators with gain. *Opt. Expr.*, **15**(26):17783-17797. [doi:10.1364/OE.15.017783]

Iwatsuki, K., Hotate, K., Higashiguchi, M., 1984. Effect of Rayleigh backscattering in an optical passive ring-resonator gyro. *Appl. Opt.*, **23**(21):3916-3924. [doi:10.1364/AO.23.003916]

Iwatsuki, K., Saruwatari, M., Kawachi, M., Yamazaki, H., 1989. Waveguide-type optical passive ring-resonator gyro using time-division detection scheme. *Electron. Lett.*, **25**(11):688-689. [doi:10.1049/el:19890465]

Leeb, W.R., Schiffner, G., Scheiterer, E., 1979. Optical fiber gyroscopes: Sagnac or Fizeau effect? *Appl. Opt.*, **18**(9):1293-1295. [doi:10.1364/AO.18.001293]

Ma, H.L., Zhang, X.L., Jin, Z.H., Ding, C., 2006. Waveguide-type optical passive ring resonator gyro using phase modulation spectroscopy technique. *Opt. Eng.*, **45**(8): 080506. [doi:10.1117/1.2280645]

Ma, H.L., He, Z.Y., Hotate, K., 2009. Sensitivity improvement of waveguide-type optical passive ring resonator gyroscope by carrier suppression. *SPIE*, **7503**:750353. [doi:10.1117/12.835029]

Ma, H.L., He, Z.Y., Hotate, K., 2011. Reduction of backscattering induced noise by carrier suppression in waveguide-type optical ring resonator gyro. *J. Lightwave Technol.*, **29**(1):85-90. [doi:10.1109/JLT.2010.2092751]

Mao, H., Ma, H.L., Jin, Z.H., 2011. Polarization maintaining silica waveguide resonator optic gyro using double phase modulation technique. *Opt. Expr.*, **19**(5):4632-4643. [doi:10.1364/OE.19.004632]

Ogata, K., 2003. Modern Control Engineering (4th Ed.). Pearson Education North Asia Limited and Publishing House of Electronics Industry, HK, China, p.13-46, 159-230.

Ohtsu, M., Tabuchi, N., 1988. Electrical feedback and its network analysis for linewidth reduction of a semiconductor laser. *J. Lightwave Technol.*, **6**(3):357-369. [doi:10.1109/50.4013]

Post, E.J., 1967. Sagnac effect. *Rev. Mod. Phys.*, **39**(2):475-493. [doi:10.1103/RevModPhys.39.475]

Sanders, G.A., Prentiss, M.G., Ezekiel, S., 1981. Passive ring resonator method for sensitive inertial rotation measurements in geophysics and relativity. *Opt. Lett.*, **6**(11): 569-571. [doi:10.1364/OL.6.000569]

Suzuki, K., Takiguchi, K., Hotate, K., 1999. Reduction of backscattering-induced noise by ternary phase shift keying in resonator micro-optic gyro integrated on silica planar lightwave circuit. *Electron. Lett.*, **35**(13):1076-1077. [doi:10.1049/el:19990736]

Suzuki, K., Takiguchi, K., Hotate, K., 2000. Monolithically integrated resonator microoptic gyro on silica planar lightwave circuit. *J. Lightwave Technol.*, **18**(1):66-72. [doi:10.1109/50.818908]

Vali, V., Shorthill, R.W., 1976. Fiber ring interferometer. *Appl. Opt.*, **15**(5):1099-1100. [doi:10.1364/AO.15.001099]

Vannahme, C., Suche, H., Reza, S., Ricken, R., Quiring, V., Sohler, W., 2007. Integrated Optical Ti: $LiNbO_3$ Ring Resonator for Rotation Rate Sensing. 13th European Conf. on Integrated Optics, paper WE1.

Ying, D.Q., Ma, H.L., Jin, Z.H., 2008. Resonator fiber optic gyro using the triangle wave phase modulation technique. *Opt. Commun.*, **281**(4):580-586. [doi:10.1016/j.optcom.2007.10.012]

Zhang, X.L., Ma, H.L., Jin, Z.H., Ding, C., 2006. Open-loop operation experiments in a resonator fiber-optic gyro using the phase modulation spectroscopy technique. *Appl. Opt.*, **45**(31):7961-7965. [doi:10.1364/AO.45.007961]